CHIN. PHYS. LETT. Vol. 38, No. 4 (2021) 047401

# Physical Properties Revealed by Transport Measurements for Superconducting $Nd_{0.8}Sr_{0.2}NiO_2$ Thin Films

Ying Xiang(相英)[1], Qing Li(李庆)[1], Yueying Li(李月莹)[2], Huan Yang(杨欢)[1*], Yuefeng Nie(聂越峰)[2], and Hai-Hu Wen(闻海虎)[1*]

[1]*National Laboratory of Solid State Microstructures and Department of Physics, Center for Superconducting Physics and Materials, Collaborative Innovation Center for Advanced Microstructures, Nanjing University, Nanjing 210093, China*

[2]*National Laboratory of Solid State Microstructures, Jiangsu Key Laboratory of Artificial Functional Materials, College of Engineering and Applied Sciences, Collaborative Innovation Center of Advanced Microstructures, Nanjing University, Nanjing 210093, China*

(Received 20 January 2021; accepted 8 February 2021; published online 6 April 2021)

The newly discovered superconductivity in infinite-layer nickelate superconducting films has attracted much attention, largely because their crystalline and electronic structures are similar to those of high-$T_c$ cuprate superconductors. The upper critical field can provide a great deal of information on the subject of superconductivity, but detailed experimental data are still lacking for these films. We present the temperature- and angle-dependence of resistivity, measured under different magnetic fields $H$ in $Nd_{0.8}Sr_{0.2}NiO_2$ thin films. The onset superconducting transition occurs at about 16.2 K at 0 T. Temperature-dependent upper critical fields, determined using a criterion very close to the onset transition, show a clear negative curvature near the critical transition temperature, which can be explained as a consequence of the paramagnetically limited effect on superconductivity. The temperature-dependent anisotropy of the upper critical field is obtained from resistivity data, which yields a value decreasing from 3 to 1.2 with a reduction in temperature. This can be explained in terms of the variable contribution from the orbital limit effect on the upper critical field. The angle-dependence of resistivity at a fixed temperature, and at different magnetic fields, cannot be scaled to a curve, which deviates from the prediction of the anisotropic Ginzburg–Landau theory. However, at low temperatures, the resistance difference can be scaled via the parameter $H^{\beta}|\cos\theta|$ ($\beta = 6$–1), with $\theta$ being the angle enclosed between the $c$-axis and the applied magnetic field. As the first detailed study of the upper critical field of nickelate thin films, our results clearly indicate a small anisotropy, and a paramagnetically limited effect, in terms of superconductivity, in nickelate superconductors.

DOI: 10.1088/0256-307X/38/4/047401

Superconductivity has recently been successfully detected in $Nd_{1-x}Sr_xNiO_2$ and $Pr_{1-x}Sr_xNiO_2$ thin films;[1,2] this observation is highly significant, since nickelates probably share similar electronic structures with high-$T_c$ cuprate superconductors. Until now, superconductivity has only been observed in thin films grown on $SrTiO_3$ substrates,[1–5] but has not been observed in $Nd_{1-x}Sr_xNiO_2$ bulk samples.[6,7] The superconducting transition occurs in a narrow doping range of Sr, i.e., $0.125 < x < 0.25$ in $Nd_{1-x}Sr_xNiO_2$ films. Meanwhile, both underdoped and overdoped samples seem to show a weak insulating property.[4,5] The multiband nature of the material can be experimentally demonstrated via the temperature-dependent Hall coefficient,[1,4] and electron energy loss spectroscopy results;[8] it is also supported by several theoretical calculations related to electronic structures.[9–27] In the parent compound of $NdNiO_2$, three sets of three-dimensional (3D) Fermi pockets are predicted, based on the theoretical calculations given in Refs. [13–16], i.e., a large $\alpha$ Fermi surface, contributed by the Ni-3$d_{x^2-y^2}$ orbital, and two small electron pockets ($\beta$ and $\gamma$), contributed by a mixed orbital contribution from Ni-3$d_{3z^2-r^2}$ and Nd-5$d_{3z^2-r^2}$/5$d_{xy}$ orbitals, due to a considerable hybridization effect.[23] The $\alpha$ pocket crosses the whole Brillouin zone in the $k_z$ direction in $NdNiO_2$, and behaves[13–15] as a hole and an electron pocket at the cut of $k_z = 0$ and $k_z = \pi$, respectively. Moreover, the low-energy Nd 5$d$ states have a self-doping effect with respect to the Ni-3$d_{x^2-y^2}$ orbital,[16–18] which may form a Kondo spin singlet state, rendering the electronic structure of Ni ion different to that of $Cu^{2+}$ in cuprates. With 20% Sr doping in $NdNiO_2$, theoretical calculations predict that the self-doping effect may disappear, making the material

Supported by the National Key R&D Program of China (Grant Nos. 2016YFA0300401 and 2018YFA0704202), the National Natural Science Foundation of China (Grant Nos. 12061131001, 11774153, and 1861161004), the Strategic Priority Research Program of Chinese Academy of Sciences (Grant No. XDB25000000), and the Fundamental Research Funds for the Central Universities (Grant No. 0213-14380167).

*Corresponding authors. Email: huanyang@nju.edu.cn; hhwen@nju.edu.cn

© 2021 Chinese Physical Society and IOP Publishing Ltd

more cuprate-like,[16,17] in that the shapes of the Fermi pockets change as compared with those of an undoped sample.[25–27] Near $k_z = 0$, the hole-like part of the $\alpha$ pocket becomes slightly larger in the doped sample, whereas near $k_z = \pi$, the electron-like component of the $\alpha$ pocket becomes slightly smaller.[13,25–27] The other two electron pockets shrink, or even disappear, with doping.[25–27] However, there are still two[25–27] or three[13] sets of 3D Fermi surfaces, primarily contributed by the Ni $3d$ and Nd $5d$ electrons in $Nd_{0.8}Sr_{0.2}NiO_2$. From this point of view, it is very interesting to investigate the superconducting anisotropy and the critical behavior of infinite-layer nickelate superconductors with multiband effects.

As a newly discovered superconducting system, the possible origin of its superconductivity has been discussed in several related works,[9,12,15,28–31] and its possible gap symmetry has also been discussed, based on theoretical calculations.[13,14,32,33] A recent scanning tunneling microcopy (STM) work shows that there are two types of superconducting gaps in the system:[34] a d-wave gap, with a gap maximum of about 3.9 meV, and a slightly anisotropic s-wave gap, with a gap maximum of about 2.35 meV. The presence of a d-wave gap further strengthens belief in the similarity between nickelate superconductors and cuprates. In most superconductors,[35] the superconducting gap $\Delta$, and the pairing strength may be linked to the upper critical field, $\mu_0 H_{c2}$, via the Pippard relation, $\xi = \hbar v_F/\pi\Delta$, and $\mu_0 H_{c2} = \Phi_0/2\pi\xi^2$. Here, $\xi$ is the coherence length, $v_F$ is the Fermi velocity, and $\Phi_0$ is the flux quantum. However, in a few superconductors, Cooper pairs break, mainly due to the Zeeman-split effect,[36] while the upper critical field is dominated by the Pauli paramagnetic limit $\mu_0 H_P^{pair} = \sqrt{2}\Delta/g\mu_B$. Here, $\mu_B$ is the Bohr magneton, and $g$ is the Landé factor. Therefore, it is worthwhile to measure the upper critical field, so as to obtain information regarding the pairing strength of this new superconducting system.

In this work, we report our experimental results with respect to temperature- and angle-dependent resistivity, measured at different magnetic fields, in superconducting $Nd_{0.8}Sr_{0.2}NiO_2$ thin films. We observe a negative curvature on the $\mu_0 H_{c2}$–$T$ curves near $T_c$, where $H \parallel ab$ plane or $H \parallel c$ axis. Furthermore, we find that the angle-dependent resistivity cannot be scaled via the anisotropic Ginzburg–Landau (GL) theory. These results suggest exotic superconductive properties in $Nd_{1-x}Sr_xNiO_2$ thin films.

The $Nd_{1-x}Sr_xNiO_3$ thin films were grown on $SrTiO_3$ substrates via the reactive molecular beam epitaxy technique, with a nominal composition of $x = 0.2$. The thickness of the film is about 6 nm. The films were stored in the vacuum chamber for more than one month at ambient temperature. We then used the soft-chemistry topotactic reduction method[1,5] to remove the apical oxygen, and obtain the superconducting $Nd_{1-x}Sr_xNiO_2$ phase. At the beginning of the topotactic hydrogen procedure, a precursor $Nd_{0.8}Sr_{0.2}NiO_3$ thin film was placed in a quartz tube, together with a pellet of $CaH_2$ weighing approximately 0.5 g. The tube was evacuated and sealed before annealing at 340℃ for 100 min. There was no direct contact between the samples and the $CaH_2$ during the treatment process. Although some unknown factors seem to be influencing the properties and the reproducibility of superconductivity in the thin films, all the 5–6 pieces of film exhibited superconductivity after a gentle post-annealing under an $H_2$ atmosphere, produced by $CaH_2$. The structure of the resultant $Nd_{0.8}Sr_{0.2}NiO_2$ film is characterized by the appearance of (001) and (002) peaks in the x-ray diffraction data, measured using a Bruker D8 Advanced diffractometer. The resistivity was measured using a standard four-electrode method in a physical property measurement system (PPMS, Quantum Design) with magnetic fields of up to 9 T.

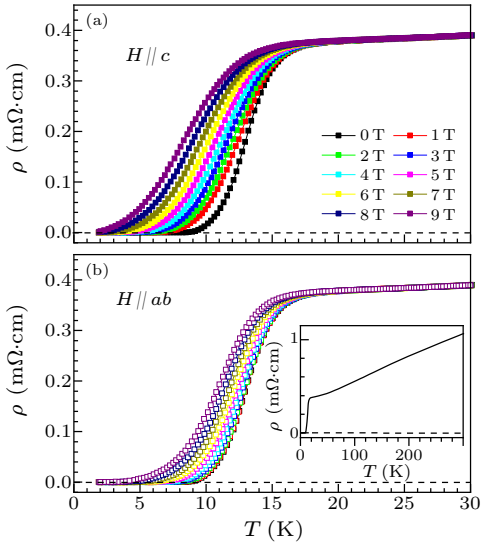


**Fig. 1.** Temperature dependence of in-plane resistivity under different magnetic fields. Temperature-dependent resistivity (current $I \parallel ab$ plane) measured in a thin film of $Nd_{0.8}Sr_{0.2}NiO_2$ at different magnetic fields ($H \perp I$), with (a) $H \parallel c$ axis and (b) $H \parallel ab$ plane, respectively. The inset in (b) shows the temperature-dependent resistivity, measured at temperatures of up to 300 K, and under 0 T.

Figure 1 shows the temperature-dependent resistivity measured at different magnetic fields, where the field is parallel or perpendicular to the $c$-axis of the film. We observe that the normal-state $\rho$–$T$ curve shows an almost linear behavior, with a positive slope in the temperature window of $20\,K < T < 30\,K$. The normal state resistivity, $\rho(T = 20\,K) = 0.38\,m\Omega{\cdot}cm$, and the corresponding residual resistance ratio $\rho(T = 300\,K)/\rho(T = 20\,K) = 2.8$ determined from the wide-temperature-range $\rho$–$T$ curve [inset in Fig. 1(b)]. Re-

sistivity curves in Fig. 1 exhibit very weak magnetoresistance in the presence of a magnetic field up to 9 T. The magnetoresistance value is only +0.16% at $T = 20$ K and $\mu_0 H = 5$ T, a value is similar to that observed in a previous work.[4] A negative Hall coefficient, $R_{\rm H} = -(2.7 \pm 0.3) \times 10^{-3}\,{\rm cm}^3/{\rm C}$, is obtained from the transverse resistance measurement using a standard six-electrode method at $T = 20$ K, with a maximum field of 5 T. The negative Hall coefficient is different from the positive values reported previously.[4,5] The different signs of Hall coefficient may be due to the slightly different oxygen content in different films, and the sign can be easily changed in this material due to the almost-balanced charge densities of holes and electrons. Derived from the temperature-dependent resistivity measured at 0 T, and shown in Fig. 1, the onset superconducting transition temperature $T_{\rm c}^{\rm onset}$ at 0 T is about 16.2 K, as determined by the criterion of $95\%\rho_{\rm n}(T)$; $\rho_{\rm n}(T)$ is the linear extrapolation of the normal-state resistivity at temperatures from 20 to 30 K. The zero-resistance transition temperature $T_{\rm c0}$ is about 9.3 K, as determined via the criterion $1\%\rho_{\rm n}(T)$. Here, the transition width is about 7 K, as determined from the $\rho$–$T$ curve, measured at 0 T, in the film. There are two possible reasons for such a broad transition in the zero field: either significant number of disorders, or a very non-mean-field transition, which would point towards an unconventional superconductivity. Since films are usually much more disordered than single crystals, the effect of inhomogeneity or disorder may be the primary reason for such a broad transition in the films examined here. This would lead to inhomogeneous superconducting phases with different $T_{\rm c}$ in the films, a hypothesis supported by the large normal-state residual resistivity of the film.

In Fig. 1, we note that the transition temperature decreases, and the transition width widens, when the magnetic field is applied in two perpendicular directions. In order to conduct a quantitative analysis of field-dependent critical temperatures, we attempt to obtain the values of zero-resistance transition fields $\mu_0 H_0$ and $\mu_0 H_{\rm c2}$, based on the $\rho$–$T$ curves, using different criteria. Figures 2(a) and 2(b) exhibit temperature-dependent characteristic fields. In our view, the zero-resistance transition fields, $\mu_0 H_0$, are determined by those superconducting phases with the lowest $T_{\rm c}$, and is also possibly affected by some weak-link behavior between different superconducting regions. Therefore, it is difficult to obtain reliable information with respect to the irreversibility field, $\mu_0 H_{\rm irr}$, from the data using a small resistivity criterion. However, the upper critical field, obtained using a high value resistivity criterion, should be dominated by superconducting phases with the highest $T_{\rm c}$, and such phases should therefore hold the strongest upper critical field. As such, the nature of the upper critical field should be intrinsic.

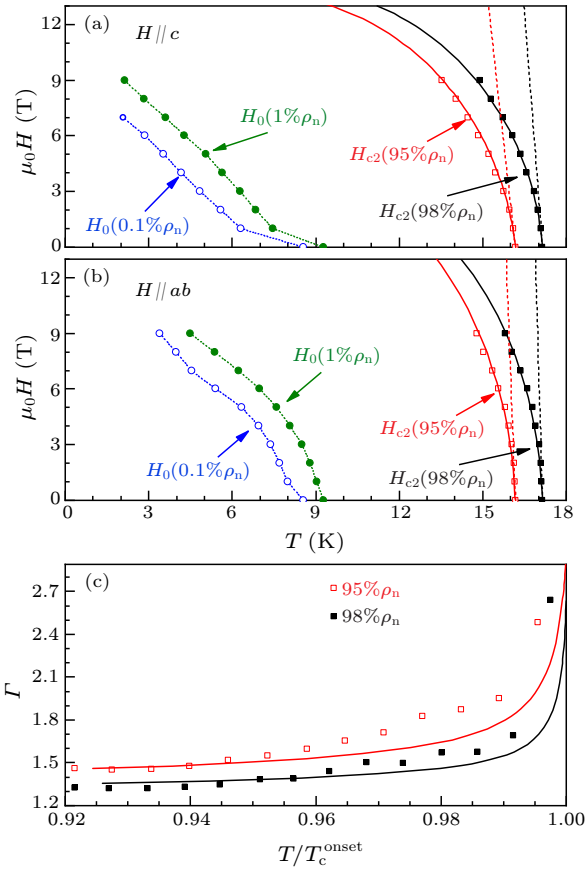


**Fig. 2.** Superconducting phase diagram and superconducting anisotropy. Symbols in (a) and (b) denote the temperature-dependent $\mu_0 H_0$ and $\mu_0 H_{\rm c2}$ obtained from $\rho$–$T$ curves, measured at different fields, and the solid (dashed) lines show the fitting results (theoretical curves) obtained from the WHH theory with finite (zero) values of $\alpha_{\rm M}$.$\mu_0 H_0$ values are determined using the criteria $0.1\%\rho_{\rm n}(T)$, and $1\%\rho_{\rm n}(T)$, while $\mu_0 H_{\rm c2}$ values are determined using the criteria $95\%\rho_{\rm n}(T)$, and $98\%\rho_{\rm n}(T)$. A clear negative curvature can be observed on the $\mu_0 H_{\rm c2}(T)$ curves near the onset transition temperature. The solid lines show the fitting results to the $\mu_0 H_{\rm c2}$–$T$ data, using the WHH theory [Eq. (1)], and assuming the absence of spin-orbital interaction ($\lambda_{\rm SO} = 0$); the values of $\alpha_{\rm M}$ are listed in Table 1. The dashed lines represent the curves of the WHH theory, where $\lambda_{\rm SO} = 0$, and $\alpha_{\rm M} = 0$. (c) The temperature dependence of the anisotropy ratio, $\Gamma(T) = H_{\rm c2}^{H\|ab}/H_{\rm c2}^{H\|c}$, (symbols) is calculated based on the $\mu_0 H_{\rm c2}$ data in (a) and (b), and the solid lines represent $\Gamma$ values derived from the fitting curves in (a) and (b).

It is evident that the slopes of the $\mu_0 H_{\rm c2}$–$T$ curves are huge near to $T_{\rm c}$. In addition, we observe in Figs. 2(a) and 2(b) that the slope $\mu_0 dH_{\rm c2}$–$dT$ decreases with an increase in temperature in the both the $H \parallel c$ axis and the $H \parallel ab$ plane, demonstrating a clear negative curvature of $H_{\rm c2}(T)$. It is understood that in a 2D superconducting system, $\mu_0 H_{\rm c2} \propto (1 - T/T_{\rm c})^{1/2}$ may appear when the magnetic field is parallel to the film plane,[37] which certainly leads to a negative curvature. However, the negative curvature does not ap-

pear close to $T_c$ when the field is perpendicular to the film.[37] Based on our data, the negative curvature appears on the $\mu_0 H_{c2}$–$T$ curves when magnetic field is either along, or perpendicular to, the film plane, which excludes the possibility of 2D superconductivity. We also conduct our investigation using experimental data from previous reports[1,5] where the magnetic field is perpendicular to the films ($H \parallel c$ axis), finding that similar negative curvatures are obtained near $T_c$ on the $\mu_0 H_{c2}$–$T$ curves, on the basis of a criterion of $95\%\rho_n(T)$ (data and treatment not shown here). In these previous works,[1,5] the film thicknesses measured 11 nm and 35 nm, respectively; this implies that negative curvature seems to be a common feature in this material, even when the magnetic field is along the $c$-axis of the sample.

Since the normal-state residual resistivity is large for this film, we attempt to use the Werthamer, Helfand, and Hohenberg (WHH) theory[36] in a dirty limit for a superconductor with a single s-wave gap, to fit our experimental data. The upper critical field can then be derived based on the WHH theory[36] via

$$\ln\frac{1}{t} = \sum_{\upsilon=-\infty}^{\infty}\left\{\frac{1}{|2\upsilon+1|} - \left[|2\upsilon+1| + \frac{\bar{h}}{t} + \frac{(\alpha_M \bar{h}/t)^2}{|2\upsilon+1| + (\bar{h}+\lambda_{SO})/t}\right]^{-1}\right\}. \quad (1)$$

Here, $t = T/T_c$; $\bar{h} = 4\mu_0 H_{c2}(T)/(\pi^2 H' T_c)$, with $H' = \mu_0|dH_{c2}/dT|_{T_c}$; $\lambda_{SO}$ is the parameter representing the strengths of the spin-orbit interaction; $\alpha_M = \sqrt{2}H_{orb}/H_P$ is the ratio of the orbital limit, $H_{orb}$, over the paramagnetic limit $H_P$, describing the contribution ratio between the pairing-breaking Zeeman energy, and the orbital pair-breaking energy.[38,39] We try to calculate $H'$ using $\mu_0 H_{c2}(T)$ data obtained at fields of 0 and 1 T, thereby obtaining the values given in Table 1. By assuming the absence of spin-orbital interaction ($\lambda_{SO} = 0$), and in the situation where $\alpha_M = 0$, we can plot the theoretical curves of $\mu_0 H_{c2}(T)$ purely contributed by the orbital. These curves are shown as dashed lines in Figs. 2(a) and 2(b). We note the almost linearly temperature-dependent upper critical field in the displayed range; this approximately linear behavior can be observed in the fitting curve when the temperature is between $0.7T_c$ and $T_c$, based on previous theoretical calculations.[36,40] However, the linear part of the experimentally obtained $\mu_0 H_{c2}(T)$ data is really very narrow, which clearly deviates from the theoretical curves where the upper critical field is contributed only by the orbital. The orbital-limited upper critical field can be calculated using the empirical formula $\mu_0 H_{orb}(0) = -0.69 T_c H'$, in the dirty limit,[40] which is equivalent to using Eq. (1) to obtain the upper critical field in the zero temperature limit under the condition of $\alpha_M = 0$. The calculated values of $\mu_0 H_{orb}(0)$ are listed in Table 1. Although the experimental data clearly deviates from the theoretical model when $\alpha_M = 0$, one can still obtain the orbital limit, $\mu_0 H_{orb}(0)$, from the slope, $H'$, at temperatures very close to $T_c$, based on previous theoretical work.[36] The anisotropic ratio in Table 1 is defined as $\Gamma = H_{c2}^{H\parallel ab}/H_{c2}^{H\parallel c}$, with $H_{c2}^{H\parallel ab}$ and $H_{c2}^{H\parallel c}$ representing the upper critical fields along the $ab$-plane and $c$-axis, respectively. These anisotropic ratios are not very large, and the value is near the upper limit of the measured data [Fig. 2(c)].

**Table 1.** $\mu_0 H_{c2}(0)$ and $\Gamma$, calculated based on the WHH theory. The fitting is performed in the absence of spin-orbit scattering. Error bars of $H'$ are determined based on both the temperature uncertainty, and errors occurring in the process of establishing $H_{c2}(T)$: the error bars of $\alpha_M$ are determined by the parameter ranges within which theoretical curves fit well with the experimental data, and the error bars of $\mu_0 H_{c2}^{orb}(0)$, $\mu_0 H_P(0)$, and $\Gamma_P(0)$ are determined via the error transfer formula.

| Criterion | $T_c^{onset}$ | Field direction | $H'$ | $\mu_0 H_{c2}^{orb}(0)$ | $\Gamma_{orb}(0)$ | $\alpha_M$ | $\mu_0 H_P(0)$ | $\Gamma_P(0)$ |
|---|---|---|---|---|---|---|---|---|
| $98\%\rho_n(T)$ | 17.1 K | $H \parallel c$ axis | $19.9 \pm 0.7$ T/K | $235 \pm 9$ T | $2.63 \pm 0.2$ | $20 \pm 1$ | $16.6 \pm 0.8$ T | $1.25 \pm 0.09$ |
| | | $H \parallel ab$ plane | $52.4 \pm 3.5$ T/K | $619 \pm 42$ T | | $42 \pm 2$ | $20.8 \pm 1.0$ T | |
| $95\%\rho_n(T)$ | 16.2 K | $H \parallel c$ axis | $13.4 \pm 0.3$ T/K | $149 \pm 4$ T | $2.97 \pm 0.16$ | $13 \pm 0.5$ | $16.2 \pm 0.6$ T | $1.29 \pm 0.08$ |
| | | $H \parallel ab$ plane | $39.7 \pm 2.0$ T/K | $443 \pm 23$ T | | $30 \pm 1.5$ | $20.9 \pm 1.0$ T | |

Since the WHH theory with $\alpha_M = 0$ cannot agree with the experimental data of $\mu_0 H_{c2}(T)$, we then try to fit the data with the only fitting parameter of $\alpha_M$ by assuming $\lambda_{SO} = 0$. Here, $H'$ has already been obtained, as mentioned above. We note that the solid lines in Figs. 2(a) and 2(b) fit the experimental data well, and the obtained $\alpha_M$ is very large in the material. Using the values of $\mu_0 H_{orb}(0)$ and $\alpha_M$, we can also obtain the values of $\mu_0 H_P(0)$, as given in Table 1. The upper critical field is in the zero-temperature limit,[36] $H_{c2}(0) = H_{orb}(0)$, when $\alpha_M \to 0$, while $H_{c2}(0) = H_P(0)$ when $\alpha_M \to \infty$. The relatively small value of $\mu_0 H_P$ may confirm that paramagnetic pair breaking dominates the upper critical field in the sample. The anomalous negative curvature on the $\mu_0 H_{c2}$–$T$ curve near $T_c$, as well as large the value of $\alpha_M$, may suggest a dominant paramagnetic pair breaking effect in the thin films used here, which is similar to the situation with other paramagnetically limited superconductors.[41–57] In addition, the obtained value of $\alpha_M$ is far larger even than those obtained in most heavy-fermion and organic

superconductors.[43–49,54] A very large value of $\alpha_{\rm M}$ indicates a dramatic mismatch between $H_{\rm orb}$ and $H_{\rm P}$. It also indicates the possible existence of the Fulde–Ferrell–Larkin–Ovchinnikov (FFLO) state[58,59] in the high-magnetic-field region at low temperatures, where the magnetic field plays a more influential role in breaking the spin-pairing. Since the FFLO state is fragile in the presence of disorder,[54] the existence of this state in the $Nd_{0.8}Sr_{0.2}NiO_2$ thin film requires further investigation via high-magnetic-field experiments.

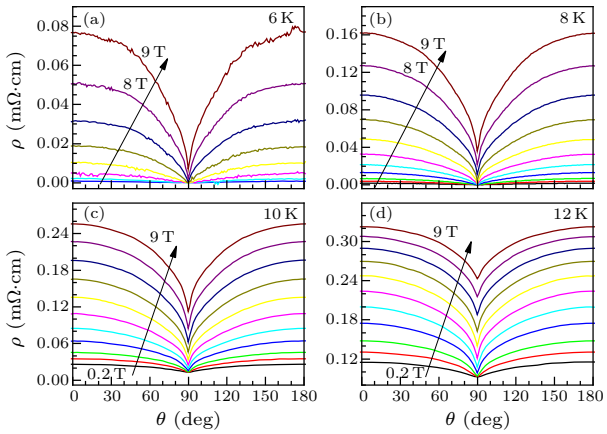


**Fig. 3.** Angular dependent resistivity, measured at different magnetic fields and temperatures in an $Nd_{0.8}Sr_{0.2}NiO_2$ thin film. The direction $\theta = 0°$, or 180°, corresponds to the direction of $H \parallel c$ axis, while $\theta = 90°$ corresponds to that of the $H \parallel ab$ plane. Magnetic fields measure (a) from 2 to 9 T, with an increment of 1 T, (b)–(d) 0.2, 0.5 T, and from 1 to 9 T, with an increment of 1 T.

The anisotropic upper critical field can usually be observed in angle-resolved resistivity data. In Fig. 3, we show the angle-dependence of resistivity, measured at different temperatures and magnetic fields. In contrast with the data measured in other systems, the resistivity dip near $\theta = 90°$ ($H \parallel ab$ plane) is very sharp. Based on the anisotropic GL theory,[35] the angle-dependence of the orbital-limiting upper critical field can be expressed as

$$H_{\rm c2}(\theta) = \frac{H_{\rm c2}^{H\parallel c}}{\sqrt{\cos^2\theta + \Gamma^{-2}\sin^2\theta}}. \qquad (2)$$

The angle-resolved resistivity can then be scaled[60] with the effective field $\tilde{H} = H\sqrt{\cos^2\theta + \Gamma^{-2}\sin^2\theta}$ by adjusting the anisotropic ratio, $\Gamma$. The theory has been successfully verified in iron-based[61,62] and $BiS_2$-based[63] superconductors of very different anisotropy ratios. In the scaling procedure, the scaled curves should coincide with the field-dependent resistivity where $H \parallel c$ axis ($\theta = 0$), given that $\tilde{H} = H$ in this situation.[64] It should be noted that the anisotropic GL theory is derived from the anisotropic vortex pinning strength,[60] but the anisotropic orbital limiting upper critical field is used in the scaling process. As mentioned above, the upper critical field may be dominated by the Pauli paramagnetic limit in $Nd_{0.8}Sr_{0.2}NiO_2$ thin films, and as such, we want to discover whether or not the anisotropic GL theory can describe the angle-dependence of resistivity in the vortex-pinning scenario. However, the scaling is not successful for any value of $\Gamma$. One set of examples of failed fittings is shown in Fig. 4, where $\Gamma = 2$, and it is impossible to make all the curves scale together; the scaling curves deviate from the $\rho$–$H$ curve, where $\theta = 0$. From this perspective, our results clearly deviate from the standard anisotropic GL scaling theory.

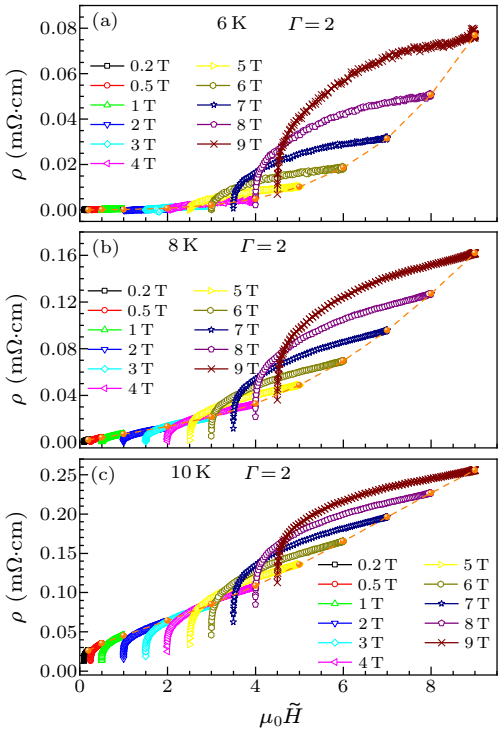


**Fig. 4.** Scaling results based on the anisotropic GL theory. Examples of failed scaling results for the $\rho$–$\theta$ curves, using the anisotropic GL theory. Here, $\tilde{H} = H\sqrt{\cos^2\theta + \Gamma^{-2}\sin^2\theta}$. Dashed lines connecting orange spherical symbols show the resistivity measured at $\theta = 0°$; the scaling curves should coincide with these lines if the anisotropic GL theory has worked.

This failed scaling behavior has been found in repeated experiments measured in the other two films. The first possible reason for the failed scaling may be the presence of inhomogeneous superconducting phases in the film. The second possibility may be that there are 2 or 3 sets of Fermi surfaces with different anisotropies[13,25–27] in the material, while the scaling model is only assumed to be applicable in the single band situation. The third possibility may be that the film is very thin, which would affect the parallel component of $\mu_0 H_{\rm c2}$, thereby contributing to the angular dependence of $\mu_0 H_{\rm c2}$, particularly at temperatures near $T_{\rm c}$, where the coherence length diverges.

However, it should be noted that Eq. (2) is used to describe the anisotropic behavior of the orbital limiting upper critical field $\mu_0 H_{c2}^{orb}(\theta)$; therefore, it is natural that the scaling does not work, because the upper critical field is dominated by the paramagnetic limit $\mu_0 H_P$ in this instance.

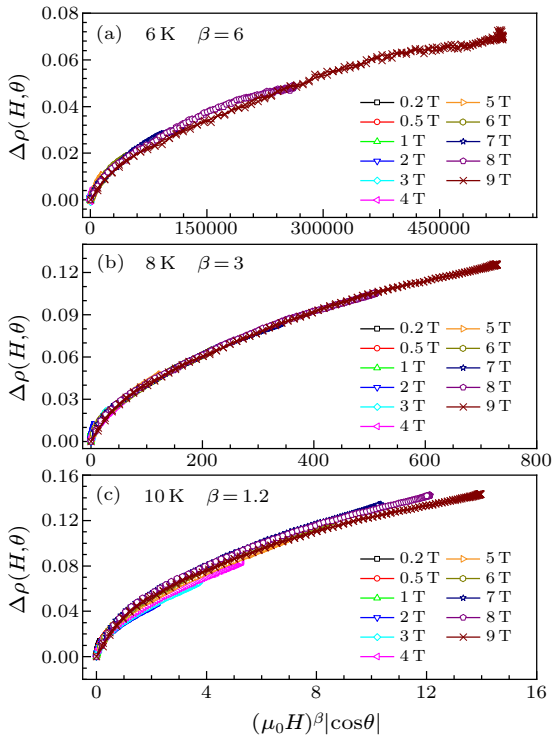


**Fig. 5.** Scaling results based on a new scaling method. Scaling results for the resistivity difference $\Delta\rho(H,\theta) = \rho(H,\theta) - \rho(H,\theta = \pi/2)$ versus $(\mu_0 H)^{\beta}|\cos\theta|$ at different temperatures.

It is difficult to obtain a simple function of $H_{c2}(\theta)$ in the paramagnetically limited system,[41] so we try to scale the measured data in other ways. Here, we use a new scaling parameter, $(\mu_0 H)^{\beta}|\cos\theta|$, to scale the increased resistivity in the magnetic field $\Delta\rho(H,\theta) = \rho(H,\theta) - \rho(H,\theta = \pi/2)$. The scaling results are presented in Fig. 5. The new scaling law seems to work well for the data taken at 6 and 8 K, although $\beta$ decreases with an increase in temperature. Scaling deteriorates at 10 K, and fails entirely for data measured at higher temperatures. The applicability of the new scaling law confirms the failure of scaling by means of the anisotropic GL theory; in the latter, a zero resistance should appear, ramping gradually due to the dissipation of vortex motion near the angle $\theta = \pi/2$. It seems that the $c$-axis component of the external magnetic field is more influential in enhancing resistivity than can be anticipated by the anisotropic GL theory. The new scaling proposal given in Fig. 5 is just a surprising empirical discovery, requiring theoretical underpinning and further studies using higher-quality samples, such as single crystals.

In superconducting $Nd_{0.8}Sr_{0.2}NiO_2$ films, we observe a negative curvature in the $\mu_0 H_{c2}$–$T$ curves near $T_c$ when the magnetic field is parallel to the $ab$-plane or the $c$-axis, and the angular-dependent resistivity measured at different fields cannot be scaled according to the anisotropic GL theory. These features have been found in three superconducting films. Since this negative curvature appears in the $\mu_0 H_{c2}$–$T$ curves when the magnetic field is along the $c$-axis, based on both our data and previously reported data[1,5] measured in films with different thicknesses from 6 to 35 nm, this contradicts the expectation for a 2D superconducting sample (as argued above); as such, the possibility of 2D superconductivity may be excluded. There are two possible reasons for this interpretation of the experimental results. One is the inhomogeneity of the film. In this case, the transition width is large, and the film may comprise different superconducting phases with distinct $T_c$ values. However, we argue that the upper critical fields determined by the method adopted here for $Nd_{0.8}Sr_{0.2}NiO_2$ films still reflect the intrinsic properties of the sample. This statement is based on the following arguments: (1) Given the inhomogeneity of the film, the upper critical field obtained using a high value of resistivity criterion (e.g., $98\%\rho_n$) should be dominated by the superconducting phase with the highest $T_c$, and this phase should hold the strongest upper critical field. (2) The negative curvature in the $\mu_0 H_{c2}$–$T$ curves near $T_c$ can also be observed in other two sets of reported data from different groups,[1,5] we can therefore conclude that this feature is related to the intrinsic superconducting mechanism of the material. The second possibility arising from our observations is that both the upper critical field, and the field-induced resistivity, are determined by the Zeeman pair-breaking effect. In this situation, the upper critical field in the paramagnetic limit can be estimated based on the binding energy of Cooper pairs, i.e., $\mu_0 H_P^{pair} = \sqrt{2}\Delta/g\mu_B$. Based on our recent STM work,[34] two superconducting gaps may open in different Fermi surfaces, with gap functions reading $\Delta_d = 3.9\cos(2\phi)$ meV (a d-wave gap), and $\Delta_s = 2.35[0.15\cos(4\phi) + 0.85]$ meV (a slightly anisotropic s-wave gap), respectively. Averaged gap values determined by $\overline{\Delta}^2 = \frac{1}{2\pi}\int_0^{2\pi}\Delta^2(\phi)d\phi$ are $\overline{\Delta_d} = 2.76$ meV, and $\overline{\Delta_s} = 2.01$ meV. By assuming a Landé factor of $g = 2$ for free electrons, the corresponding $\mu_0 H_{P\,d}^{pair} = 21$ T, and $\mu_0 H_{P\,s}^{pair} = 15$ T, respectively. These estimated values of paramagnetic limits are very close to the fitting results given in Table 1. It should be noted that an estimation based on the single gap model is very crude with respect to this complex material, but the estimation results justify our analysis here.

A related observation is the incredibly large value of $\alpha_M$ obtained from the fittings. The reason for the large $\alpha_M$ value in heavy-fermion superconductors

is due to their large effective mass. Based on the single-band model in the clean limit of the Bardeen–Cooper–Schrieffer (BCS) theory, the Maki parameter $\alpha_{\rm M} \propto m\Delta/E_{\rm F}$ when $H \parallel c$ axis.[38,39] A very large value of $\alpha_{\rm M}$ corresponds to a very large effective mass, $m$, and/or a very small Fermi energy, $E_{\rm F}$. Currently, however, both parameters are lacking with regard to superconducting nickelate films. Theoretically, it has been suggested in Ref. [18] that the Nd-5$d$ conduction electrons may couple to localized Ni-3$d_{x^2-y^2}$ electrons to form Kondo spin singlets, leading to an enhanced effective mass at low temperatures. The above discussions are based on the single-gap model, whereas in truth, we are dealing with a multiband superconductor, which tends to make any analysis more complicated. For example, there are many more fitting parameters to fit the $\mu_0 H_{c2}$–$T$ data in the multi-gap situation than in the single-gap scenario.[57,65] A good fitting by a multi-gap model requires more data relating to $\mu_0 H_{c2}$–$T$, measured at much higher fields and at low temperatures. Therefore, it would be highly advantageous to measure the upper critical field directly at low temperatures and high magnetic fields in future works.

A further observation arising from our experiments is that the anisotropy ratio is not large for either $\mu_0 H_{\rm P}$ or $\mu_0 H_{\rm orb}$, in these films. The obtained $\Gamma$ is in the range of 1.2 to 3.0, as derived from the experimental data in Fig. 2(c), while $\Gamma_{\rm orb}(0)$ is about 2.3–2.97, based on the fittings. The anisotropy ratio is comparable to those found in iron-based superconductors,[66] but much smaller than those found in cuprates, such as the Bi-2212 system[35] or $BiS_2$-based[63] superconductors. It should be noted that the $Nd_{1-x}Sr_xNiO_2$ material is in the infinite-layer phase; as such, a small anisotropy value is predictable. In addition, many theoretical calculations[13,25–27] have demonstrated the presence of a large $\alpha$ Fermi surface with a strong dispersion along the $k_z$-axis in $Nd_{0.8}Sr_{0.2}NiO_2$; moreover, there are still one[25–27] or two[13] small 3D electron Fermi pockets, all of which would lead to a low anisotropy. Based on the picture of a paramagnetically dominated superconductivity, $\Gamma_{\rm P}(0)$ is only about 1.25–1.29 from the fitting, suggesting a small anisotropy of Pauli susceptibilities or $g$ factors along the two perpendicular axes.[41] The increase in anisotropy with temperature in Fig. 2(c) can be explained by the increased contribution from the orbital limit when the temperature approaches $T_{\rm c}$. The orbital limiting effect dominates the upper critical field near $T_{\rm c}$, and generally results in a relatively larger anisotropy. On the contrary, in the low temperature region, the Pauli limit should give a relatively smaller anisotropy, play an increasingly important role, and finally become decisive in determining the upper critical field. This would explain the strong temperature dependence of the anisotropy of measured upper critical fields.

In summary, we have conducted resistive transport measurements under magnetic fields in superconducting thin films of $Nd_{0.8}Sr_{0.2}NiO_2$, with an onset superconducting transition temperature of about 16.2 K. The anisotropy of the measured upper critical field is small, located in the range of 1.2 to 3 near the transition temperature. We observe a negative curvature of the $\mu_0 H_{c2}$–$T$ curve near $T_{\rm c}$, which is interpreted as a possible consequence of paramagnetic limited superconductivity. The angle-dependence of resistivity at a fixed temperature and different magnetic fields cannot be scaled using the anisotropic Ginzburg–Landau theory. We have found that the enhanced resistivity is strongly influenced by the $c$-axis component of the magnetic field. This may be induced either by paramagnetically limited superconductivity, or by inhomogeneity in the films. Our observations provide useful information with respect to this newly discovered infinite-layer nickelate superconducting system.

*Supporting note added*: While this work was under review, a new manuscript was posted on arXiv. It reports similar transport measurements in an $Nd_{0.775}Sr_{0.225}NiO_2$ thin film. The authors reached the same conclusion as ourselves, i.e., that the upper critical field is determined by the paramagnetic limiting effect.[67]

## References


[1] Li D, Lee K, Wang B Y, Osada M, Crossley S, Lee H R, Cui Y, Hikita Y and Hwang H Y 2019 *Nature* **572** 624
[2] Osada M, Wang B Y, Goodge B H, Lee K, Yoon H, Sakuma K, Li D, Miura M, Kourkoutis L F and Hwang H Y 2020 *Nano Lett.* **20** 5735
[3] Lee K, Goodge B H, Li D, Osada M, Wang B Y, Cui Y, Kourkoutis L F and Hwang H Y 2020 *APL Mater.* **8** 041107
[4] Li D, Wang B Y, Lee K, Harvey S P, Osada M, Goodge B H, Kourkoutis L F and Hwang H Y 2020 *Phys. Rev. Lett.* **125** 027001
[5] Zeng S, Tang C S, Yin X, Li C, Huang Z, Hu J, Liu W, Omar C J, Jani H, Lim Z S, Han K, Wan D, Yang P, Wee A T S and Ariando A 2020 *Phys. Rev. Lett.* **125** 147003
[6] Li Q, He C, Si J, Zhu X, Zhang Y and Wen H H 2020 *Commun. Mater.* **1** 16
[7] Wang B X, Zheng H, Krivyakina E, Chmaissem O, Lopes P P, Lynn J W, Gallington L C, Ren Y, Rosenkranz S, Mitchell J F and Phelan D 2020 *Phys. Rev. Mater.* **4** 084409
[8] Goodge B H, Li D, Lee K, Osada M, Wang B Y, Sawatzky G A, Hwang H Y and Kourkoutis L F 2021 *Proc. Natl. Acad. Sci. USA* **118** e2007683118
[9] Nomura Y, Hirayama M, Tadano T, Yoshimoto Y, Nakamura K and Arita R 2019 *Phys. Rev. B* **100** 205138
[10] Choi M Y, Lee K W and Pickett W E 2020 *Phys. Rev. B* **101** 020503(R)
[11] Botana A S and Norman M R 2020 *Phys. Rev. X* **10** 011024
[12] Zhou T, Gao Y and Wang Z D 2020 *Sci. Chin. Phys. Mech. & Astron.* **63** 287412
[13] Wu X, Sante D D, Schwemmer T, Hanke W, Hwang H Y, Raghu S and Thomale R 2020 *Phys. Rev. B* **101** 060504(R)
[14] Adhikary P, Bandyopadhyay S, Das T, Dasgupta I and Saha-Dasgupta T 2020 *Phys. Rev. B* **102** 100501(R)

[15] Liu Z, Ren Z, Zhu W, Wang Z and Yang J 2020 *npj Quantum Mater.* **5** 31
[16] Lechermann F 2020 *Phys. Rev. B* **101** 081110(R)
[17] Krishna J, LaBollita H, Fumega A O, Pardo V and Botana A S 2020 *Phys. Rev. B* **102** 224506
[18] Zhang G M, Zhang Y and Zhang F C 2020 *Phys. Rev. B* **101** 020501(R)
[19] Sakakibara H, Usui H, Suzuki K, Kotani T, Aoki H and Kuroki K 2020 *Phys. Rev. Lett.* **125** 077003
[20] Zhang H, Jin L, Wang S, Xi B, Shi X, Ye F and Ming J W 2020 *Phys. Rev. Res.* **2** 013214
[21] Lechermann F 2020 *Phys. Rev. X* **10** 041002
[22] Petocchi F, Christiansson V, Nilsson F, Aryasetiawan F and Werner P 2020 *Phys. Rev. X* **10** 041047
[23] Lee K W and Pickett W E 2004 *Phys. Rev. B* **70** 165109
[24] Wan X, Ivanov V, Resta G, Leonov I and Savrasov S Y 2021 *Phys. Rev. B* **103** 075123
[25] Wang Y, Kang C J, Miao H and Kotliar J 2020 *Phys. Rev. B* **102** 161118(R)
[26] Kang C J and Kotliar G 2020 arXiv:2007.15383 [cond-mat.str-el]
[27] Karp J, Hampel A, Zingl M, Botana A S, Park H, Norman M R and Millis A J 2020 *Phys. Rev. B* **102** 245130
[28] Hepting M, Li D, Jia C J, Lu H, Paris E, Tseng Y, Feng X, Osada M, Been E, Hikita Y, Chuang Y D, Hussain Z, Zhou K J, Nag A, Garcia-Fernandez M, Rossi M, Huang H Y, Huang D J, Shen Z X, Schmitt T, Hwang H Y, Moritz B, Zaanen J, Devereaux T P and Lee W S 2020 *Nat. Mater.* **19** 381
[29] Ryee S, Yoon H, Kim T J, Jeong M Y and Han M J 2020 *Phys. Rev. B* **101** 064513
[30] Hu L H and Wu C 2019 *Phys. Rev. Res.* **1** 032046(R)
[31] Gu Y, Zhu S, Wang X, Hu J and Chen H 2020 *Commun. Phys.* **3** 84
[32] Zhang Y H and Vishwanath A 2020 *Phys. Rev. Res.* **2** 023112
[33] Wang Z, Zhang G M, Yang Y and Zhang F C 2020 *Phys. Rev. B* **102** 220501(R)
[34] Gu Q, Li Y, Wan S, Li H, Guo H, Yang H, Li Q, Zhu X, Pan X, Nie Y and Wen H H 2020 *Nat. Commun.* **11** 6027
[35] Tinkham M 1996 *Introduction to Superconductivity* 2nd edn (New York: McGraw-Hill, Inc)
[36] Werthamer N R, Helfand E and Hohenberg P C 1966 *Phys. Rev.* **147** 295
[37] Ruggiero S T, Barbee T W and Beasley M R 1980 *Phys. Rev. Lett.* **45** 1299
[38] Sarma G 1963 *J. Phys. Chem. Solids* **24** 1029
[39] Maki K 1966 *Phys. Rev.* **148** 362
[40] Helfand E and Werthamer N R 1966 *Phys. Rev.* **147** 288
[41] Brison J P, Keller N, Vernière A, Lejay P, Schmidt L, Buzdin A, Flouquet J, Julian S R and Lonzarich G G 1995 *Physica C* **250** 128
[42] Buzdin A I and Brison J P 1996 *Europhys. Lett.* **35** 707
[43] Bianchi A, Movshovich R, Capan C, Pagliuso P G and Sarrao J L 2003 *Phys. Rev. Lett.* **91** 187004
[44] Radovan H A, Fortune N A, Murphy T P, Hannahs S T, Palm E C, Tozer S W and Hall D 2003 *Nature* **425** 51
[45] Kumagai K, Saitoh M, Oyaizu T, Furukawa Y, Takashima S, Nohara M, Takagi H and Matsuda Y 2006 *Phys. Rev. Lett.* **97** 227002
[46] Matsuda Y and Shimahara H 2007 *J. Phys. Soc. Jpn.* **76** 051005
[47] Agosta C C, Martin C, Radovan H A, Palm E C, Murphy T P, Tozer S W, Cooley J C, Schlueter J A and Petrovic C 2006 *J. Phys. Chem. Solids* **67** 586
[48] Singleton J, Symington J A, Nam M S, Ardavan A, Kurmoo M and Day P 2000 *J. Phys.: Condens. Matter* **12** L641
[49] Coniglio W A, Winter L E, Cho K, Agosta C C, Fravel B and Montgomery L K 2011 *Phys. Rev. B* **83** 224507
[50] Agosta C C, Jin J, Coniglio W A, Smith B E, Cho K, Stroe I, Martin C, Tozer S W, Murphy T P, Palm E C, Schlueter J A and Kurmoo M 2012 *Phys. Rev. B* **85** 214514
[51] Mayaffre H, Krämer S, Horvatić M, Berthier C, Miyagawa K, Kanoda K and Mitrović V F 2014 *Nat. Phys.* **10** 928
[52] Agosta C C, Fortune N A, Hannahs S T, Gu S, Liang L, Park J H and Schleuter J A 2017 *Phys. Rev. Lett.* **118** 267001
[53] Wosnitza J 2018 *Ann. Phys.* **530** 1700282
[54] Agosta C C 2018 *Crystals* **8** 285
[55] Klein T, Braithwaite D, Demuer A, Knafo W, Lapertot G, Marcenat C, Rodière P, Sheikin I, Strobel P, Sulpice A and Toulemonde P 2010 *Phys. Rev. B* **82** 184506
[56] Gurevich A 2011 *Rep. Prog. Phys.* **74** 124501
[57] Gurevich A 2010 *Phys. Rev. B* **82** 184504
[58] Fulde P and Ferrell R A 1964 *Phys. Rev.* **135** A550
[59] Larkin A I and Ovchinnikov Y N 1964 *Zh. Eksp. Teor. Fiz.* **47** 1136; [1965 *Sov. Phys. JETP* **20** 762]
[60] Blatter G, Geshkenbein V B and Larkin A I 1992 *Phys. Rev. Lett.* **68** 875
[61] Wang Z S, Luo H Q, Ren C and Wen H H 2008 *Phys. Rev. B* **78** 140501
[62] Li C H, Shen B, Han F, Zhu X Y and Wen H H 2011 *Phys. Rev. B* **83** 184521
[63] Liu J Z, Fang D L, Wang Z Y, Xing J, Du Z Y, Li S, Zhu X Y, Yang H and Wen H H 2014 *Europhys. Lett.* **106** 67002
[64] Jovanović V P, Li Z Z and Raffy H 2009 *Phys. Rev. B* **80** 024501
[65] Smylie M P, Koshelev A E, Willa K, Willa R, Kwok W K, Bao J K, Chung D Y, Kanatzidis M G, Singleton J, Balakirev F F, Hebbeker H, Niraula P, Bokari E, Kayani A and Welp U 2019 *Phys. Rev. B* **100** 054507
[66] Stewart G R 2011 *Rev. Mod. Phys.* **83** 1589
[67] Wang B Y, Li D, Goodge B H, Lee K, Osada M, Harvey S P, Kourkoutis L F, Beasley M R and Hwang H Y 2020 arXiv:2012.06560 [cond-mat.supr-con]